This paper is part of a special issue on Supersonic Jet Noise

Investigation of vortical and near-acoustic fields in three-stream jets

Andres Adam,[1] Juntao Xiong,[1] and Dimitri Papamoschou[1]

University of California, Irvine, Irvine, CA, 92697, USA

(Dated: 3 August 2021)

We investigate the connections between the vortical and near-acoustic fields of three-stream, high-speed jets for the purpose of developing linear surface-based models for the noise source. Those models would be informed by low-cost, Reynolds-Averaged Navier-Stokes (RANS) computations of the flow field. The study uses two triple-stream jets, one coaxial and the other with eccentric tertiary flow that yields noise suppression in preferred directions. Large Eddy Simulations (LES) validate RANS-based models for the convective velocity U_c of the noise-generating turbulent eddies. In addition, the LES results help define a "radiator surface" on which the jet noise source model would be prescribed. The radiator surface is located near the boundary between the rotational and irrotational fields and is defined as the surface on which the U_c distribution, obtained from space-time correlations of the pressure, matches that inferred from the RANS model. The edge of the mean vorticity field is nearly coincident with the radiator surface, which suggests a RANS-based criterion for locating this surface. Two-dimensional space-time correlations show how the asymmetry of the tertiary stream, and the resulting thicker low-speed flow, weakens the generation of acoustic disturbances from the vortical field.

I. INTRODUCTION

The research effort described here targets the development of low-cost predictive models for the noise emission of complex multi-stream turbulent jets associated with the exhaust of advanced turbofan engines. For these models to be effective as design tools, they need to rely entirely on Reynolds-Averaged Navier Stokes (RANS) solutions of the flow field. With reasonable computational resources, RANS solutions can be obtained within hours. High-fidelity methods such as large eddy simulation (LES), coupled with surface integral methods, have evolved to the point where they can yield accurate noise predictions[1]. However, they entail very large computational resources, long turnaround times, and enormous data sets. On the other hand, the analysis of LES results can help in the creation of low-order models by shedding light on the physical mechanisms of noise generation, as it is done in this work.

The present investigation considers three-stream jets at conditions relevant to variable-cycle engines for supersonic aircraft. Henderson[2] surveyed the acoustics of a three-stream configuration where the core and bypass streams are internally mixed upstream of the tertiary exit; the added tertiary flow reduced high-frequency noise at broadside and peak jet noise angles. Henderson *et al.*[3] conducted acoustic experiments and flow field simulations of jets from three-stream nozzles with axisymmetric and offset configurations for the tertiary stream. The offset tertiary stream reduced noise along the thick side of the jet when the core flow was operating at supersonic conditions. Henderson and Wernet[4] investigated the mean flow field and turbulence characteristics of externally mixed, convergent three stream nozzles using stereo particle image velocimetry. Huff *et al.*[5] assessed the capability of three-stream, offset duct configurations to meet Chapter 14 noise regulations. Our research group has conducted extensive parametric studies of offset three-stream nozzle concepts and has identified promising quiet configurations that involve duct asymmetry in combination with a wedge-shaped fan flow deflector[6,7].

RANS-based predictive models for multi-stream jets have focused on the acoustic analogy coupled with methods to account for the refraction by the mean flow. Including the refraction is particularly critical for asymmetric configurations with azimuthal directivity of the acoustic emission. Construction of the related Green's functions involves complex numerical procedures[8]. Application to three-stream jets with offset tertiary duct has shown initial promise[3], although the asymmetry in the modeled azimuthal directivity was weaker than the experimental one. More recently, Papamoschou[9] has proposed an alternative methodology where the azimuthal influence is induced by special forms of the space-time correlations of the Lighthill stress tensor. This work has also underscored the importance of properly modeling the convective velocity U_c of the turbulent eddies that dominate sound production[9]. Specifically, for velocity ratios of relevance to the exhaust of turbofan engines, sound emission is thought to be strongly influenced by the dynamics of the outer shear layer in the initial region of a multi-stream jet. Support for this observation comes from the modeling of coaxial jet noise by Tanna and Morris[10] and Fisher *et al.*[11]. A number of additional works have validated and refined this concept, including experiments on mean velocity profiles and noise source location[12] and near-field pressure measurements[13,14]. Considering the entire jet, one can generalize this observation by stating that the turbulent eddies in contact with the ambient air are the main generators of noise. In a time-averaged sense, the action of the eddies in the outer shear layer is represented by the local peak of the Reynolds stress, resulting in the definition of the outer surface of peak stress (OSPS). The mean axial velocity on this surface is set to represent U_c, and the axial convective Mach number, which controls the radiation efficiency, is defined accordingly. Related work by Bridges and Wernet[15] found that the local turbulent convection speed is roughly equal to the local mean velocity in regions with high turbulence intensity. Stuber *et al.*[16] studied an axisymmetric and an asymmetric three-stream jets and found connections between their difference in noise generation and their convective velocities. Prasad and Morris[17] studied the effect of fluidic inserts on the noise of single-stream, heated supersonic jets and attributed the noise reduction enabled by the inserts to reduced convective velocities. Daniel *et al.*[18] studied the noise emission from high-speed jets with temperature non-uniformity and measured noise reduction that was connected to a reduced convective velocity.

An alternative to the acoustic analogy is surface-based modeling where propagation starts from a Kircchoff surface located in the linear pressure field[19,20]. In the frequency domain, propagation off the surface requires knowledge of the pressure and its normal derivative on the surface. For simple surfaces (e.g., cylindrical or conical) analytical formulations of the surface Green's function can be used to propagate to the far field. For complex surfaces, the problem can be tackled numerically by a variety of methods, including the boundary element method[21]. In principle, the data on the Kircchoff surface would be determined by a time-resolved solution of the non-linear flow enclosed by the surface, which makes the approach costly. Considerable effort has been placed on developing simple models for the surface source that would alleviate this cost. In several of these models for jet noise, the surface source takes the form of pressure partial fields, each partial field being an amplitude-modulated traveling wave (wavepacket) containing hydrodynamic and acoustic components. The acoustic field can then be constructed via stochastic superposition of the pressure field emitted by each wavepacket. Such constructions can be found in Refs. 22–25. The modeling of the surface source is benefiting from fundamental works on the wavepacket modeling of jet noise that have made significant progress in the last decade[26–29]. Using the source surface approach one can predict not only propagation but also scattering from airframe surfaces[30,31], thus addressing the acoustics of propulsion-airframe integration. Surface-based models may also simplify the treatment of the azimuthal directivity from asymmetric jets noted above. The conceptual application of this approach to multi-stream jets is depicted in Fig. 1. The source is prescribed as random partial fields on a "radiator surface" at the boundary between the inner nonlinear rotational flow field and outer linear pressure field. As will be defined in this paper, the radiator surface is a unique Kirchhoff surface on which the pressure distribution reflects the footprint of the turbulence, and in particular the coherent structures that dominate mixing and noise generation[32,33]. As with the acoustic analogy approach, modeling of the convective velocity U_c on the radiator surface is a critical element of the predictive scheme.

To make this model low-cost, it desired that the radiator surface and the partial fields prescribed on it be based on a RANS solution of the flow field. The complexity of the multi-stream jet flow field makes this a challenging proposition. Before such model can be envisioned, we need to better understand and model the relation between the inner vortical field and the linear pressure field at the edge of the jet. Of particular interest is how this relation changes when asymmetry is introduced and how well RANS can capture the resulting effects. To this end, we make extensive comparisons between RANS solutions, and the models derived by it, and a time-resolved solution given by large eddy simulation (LES). Our initial aim is to establish whether RANS has the potential to inform a differential model for acoustic emission, i.e., a model that would predict the changes from a known axisymmetric baseline. The paper is organized as follows. The nozzle characteristics and their operating conditions are outlined in Section II. The details of the LES and RANS simulations are explained in Section III. Then, their results on the mean flow fields are presented in Section IV. The relevant surfaces for noise source modeling, the OSPS and the radiator surface, are studied in Sections V and VI respectively. Finally, two-dimensional space-time correlations are used to investigate noise reduction mechanisms in Section VII.

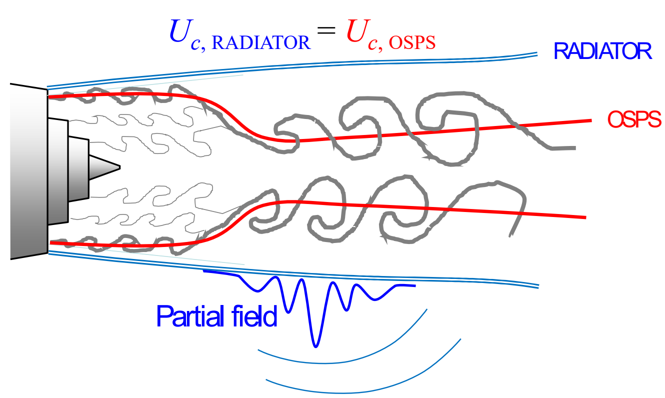

FIG. 1. Basic elements of surface-based modeling of the noise source of multi-stream jets.

II. JET FLOWS

We study the flow fields of two high-speed turbulent jets exiting from the triple-stream nozzles depicted in Fig. 2(a). The nozzles have external plugs and the mixing of the streams is external to the nozzles. The Cartesian and polar coordinate systems used here, $\mathbf{x} = (x, y, z)$ and $\mathbf{x} = (x, r, \phi)$, are illustrated in Fig. 2(b). The origin of the axial coordinate x is at the plug tip. Subscripts p, s and t refer to the primary (inner), secondary (middle) and tertiary (outer) streams, respectively. The azimuthal angle ϕ is defined relative to the downward vertical direction. Both nozzles have the same duct exit areas and plug dimensions. The effective (area-based) exit diameter of the primary duct is $D_{p,eff} = 13.33$ mm, the secondary-to-primary area ratio is $A_s/A_p = 1.44$ and the tertiary-to-primary area ratio is $A_t/A_p = 1.06$. The diameter of the tertiary duct is $D_t = 38.1$ mm. The plug diameter is 23.80 mm and its length, as measured from the primary exit plane to the plug tip, is 38.4 mm.

Nozzle AXI04U is coaxial and thus features uniform distributions of secondary and tertiary duct exit widths at $W_s/D_{p,eff} = 0.219$ and $W_t/D_{p,eff} = 0.127$, respectively. Nozzle ECC09U has the same primary and secondary ducts as AXI04U but features a tertiary duct of variable exit width $W_t(\phi)$, plotted in Fig. 2 (c). The distribution is symmetric around the plane $z = 0$. Compared to nozzle AXI04U, the tertiary duct of ECC09U is wider in the annular segment $-110^\circ < 0 < 110^\circ$ and thinner elsewhere. On the top of the nozzle, the tertiary duct closes completely by means of a wedge-type deflector of axial length of $2.1D_{p,eff}$ and half angle $\delta = 25^\circ$. This eccentric tertiary duct causes a thickened tertiary flow on the underside of the nozzle.

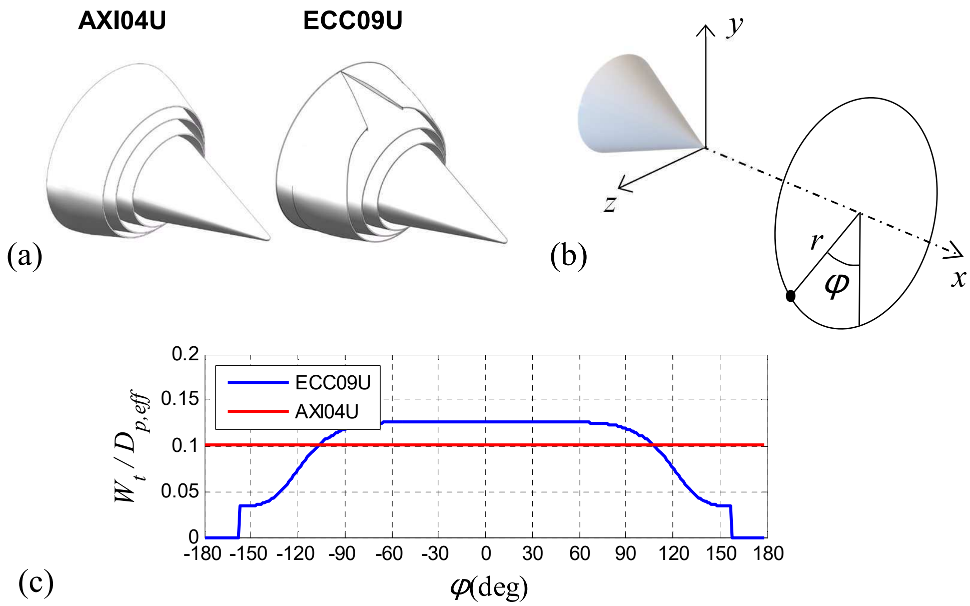

FIG. 2. (a) Exit geometry of nozzles; (b) coordinate system; (c) azimuthal variation of the tertiary annulus width.

The flow conditions are common for both nozzles and are listed in Table I. They represent typical exhaust conditions for a supersonic turbofan engine[7]. In the table, NPR is the nozzle pressure ratio, NTR is the nozzle temperature ratio, A is the exit cross-sectional area, $\dot{m}$ is the mass flow rate, M is the fully-expanded Mach number, and U is the fully-expanded velocity. The Reynolds number based on the primary exit conditions and $D_{p,eff}$ is 1.8×10^5.

Jets AXI04U and ECC09U were part of a campaign to investigate the acoustics of coaxial and asymmetric three-stream jets[7,34]. Small-scale experiments utilized helium-air mixtures to match the flow conditions shown in Table 1. To demonstrate the noise suppression ability of the eccentric tertiary flow, Fig. 3 plots the far-field narrowband spectra of jets AXI04U and ECC09U in the downward polar direction of peak emission (approximately 35° below the

Stream	NPR	NTR	A/A_p	$\dot{m}/\dot{m}_p$	M	U (m/s)
Primary	2.06	3.38	1.07	1.00	1.00	590
Secondary	2.03	1.34	1.06	2.33	1.44	370
Tertiary	1.53	1.24	0.81	1.31	1.06	282

TABLE I. Flow conditions.

jet axis)[34]. The spectra are plotted versus the laboratory frequency, which is about 50 times larger than the full-scale frequency for a supersonic business jet. The eccentricity of the tertiary duct in ECC09U yields large reductions, as much as 12 dB, at full-scale frequency in the range of 200 - 500 Hz. Understanding and modeling the physical mechanisms of this reduction motivates the research effort discussed in this paper.

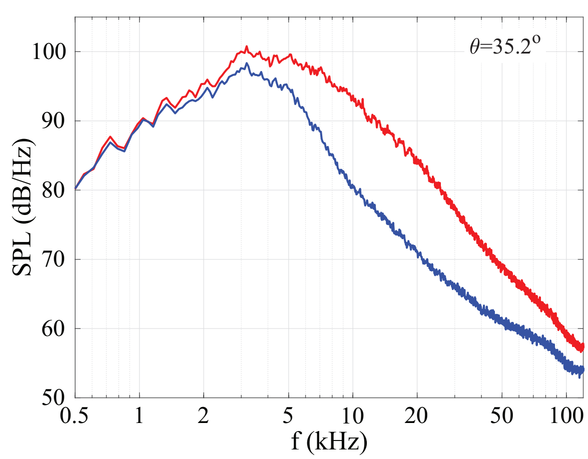

FIG. 3. Far-field sound pressure level spectra of jets AXI04U (red) and ECC09U (blue) at polar angle of 35° with respect to the downstream axis[34].

In the presentation of the results that follow, equivalent length and velocity scales will be used to properly normalize the coordinates and flow variables. The equivalent diameter $\widehat{D}$ is based on the total exit cross-sectional area and has the value of 24.9 mm. The equivalent velocity is the mass-flow-rate averaged velocity

$$\widehat{U} = \frac{\dot{m}_p U_p + \dot{m}_s U_s + \dot{m}_t U_t}{\dot{m}_p + \dot{m}_s + \dot{m}_t} \tag{1}$$

and has the value of 435 m/s.

III. COMPUTATIONAL DETAILS

The computational effort encompassed Reynolds-Averaged Navier Stokes (RANS) solutions and Large Eddy Simulations (LES) performed at the conditions of Table I and the Reynolds numbers listed in the previous section. The computational fluid dynamics code is known as PARCAE[35] and solves the unsteady three-dimensional Navier-Stokes equations on structured multiblock grids using a cell-centered finite-volume method.

The RANS computations use the Jameson-Schmidt-Turkel dissipation scheme[36] and the Shear Stress Transport (SST) turbulence model of Menter[37]. The solver has been used in past research on dual-stream jets, and its predictions have been validated against mean velocity measurements for dual-stream jets[35].

The LES computations use implicit backward three-layer second-order time integration with explicit five stage Runge-Kutta dual time stepping, residual smoothing, and multigrid techniques for convergence acceleration. The spatial discretization of the inviscid flux is based on the weighted averaged flux-difference splitting algorithm of Roe[38,39]. The viscous flux is discretized using a second-order central difference scheme. The time-evolving jet flow is simulated using a hybrid RANS/LES approach[40]. The Spalart-Allmaras turbulence model[41] is used to model the turbulent viscosity near the walls, while in the free shear flow the computation relies on the subtle dissipation of the upwind scheme, using the method proposed by Shur *et al.*[39]. Experimental mean-velocity profiles of cold jets issuing from the nozzles of this study have been well replicated by the LES predictions; in addition, LES-based predictions of far-field sound pressure level spectra (in conjunction with a Ffowcs-Williams-Hawkings surface) have reproduced satisfactorily experimental spectra for the nozzles and operating conditions of this study[42].

The computations encompassed both the internal nozzle flow as well as the external plume. At the inlet surface of each nozzle stream, the boundary conditions specified uniform total pressure and total temperature corresponding to their perfectly expanded exit Mach number. The ambient region surrounding the nozzle flow had a characteristic boundary condition, and the downstream static pressure was set to the ambient pressure. The nozzle walls had an adiabatic, no-slip boundary condition. To aid convergence, the RANS and LES simulations were conducted with a freestream Mach number of 0.05, equivalent to a velocity of 17 m/s.

For the RANS solutions, the mesh contained approximately 8 million grid points and extended to $46\widehat{D}$ axially and $12\widehat{D}$ radially. As the nozzles are symmetric around the $x-y$ plane, only one half of the nozzles and jet flows were modeled to save computational cost. The LES grids contained about 44 million grid points each and extended to $46\widehat{D}$ axially and $23\widehat{D}$ radially.

The results of nozzle AXI04U were calculated with 4100 time frames after the transient period at a time step of $\Delta t = 10$ μs, yielding a simulation time of $716\widehat{D}/\widehat{U}$. Due to limited computational resources, the simulation of ECC09U was moderately shorter at 3130 time frames with the same time step, resulting in a simulation time of $546\widehat{D}/\widehat{U}$. Given that nozzle AXI04U is axisymmetric, its results are averaged in the azimuthal direction whenever possible to improve smoothness. The same treatment is not applicable to jet ECC09U.

The LES flow field enables two-point space-time correlations throughout the domain. Considering fluctuating flow variables $a'(\mathbf{x}, t)$ and $b'(\mathbf{x}, t)$ with zero means, their normalized space-time correlation is defined by

$$R_{ab}(\mathbf{x}_0, \mathbf{x}, \tau) = \frac{\overline{a'(\mathbf{x}_0, t)\ b'(\mathbf{x}, t+\tau)}}{\left(\overline{a'(\mathbf{x}_0)^2}\ \overline{b'(\mathbf{x})^2}\right)^{1/2}} \tag{2}$$

where $\mathbf{x}_0$ is the reference location, $\mathbf{x}$ is the displaced location, τ is the time separation, and the overline denotes time averaging. Equation 2 assumes stationarity in time t. In the analysis that follows we will consider space-time correlations of the pressure fluctuation p' with itself, (R_{pp}), axial velocity fluctuation u' with itself (R_{uu}), as well as u' with p' (R_{up}).

The space-time correlations enable calculation of the convective velocity by locating the time separation where the correlation peaks. Here this calculation will be restricted to axial displacements only, with $\mathbf{x}_0 = (x_0, r_0, \phi_0)$ and $\mathbf{x} = (x_0 + \xi, r_0, \phi_0)$. The resulting axial convective velocity U_c will be based on R_{pp} and R_{uu}. Figure 4 shows an example space-time correlation. Practical implementation of the U_c measurement requires several space-time correlations at small axial separations ξ_i. Because each correlation function comprises a discrete set of points, to accurately locate the maximum value of the correlation at axial separation ξ_i a seventh-order polynomial is fitted around the peak of the correlation curve (dashed lines in Fig. 4). The time separation τ_i corresponds to the maximum value of the polynomial. The convective velocity for this axial separation is $U_{c,i} = \xi_i/\tau_i$, and the overall U_c assigned to the reference point is the average of all $U_{c,i}$ computed from correlations whose peak values exceed 0.4.

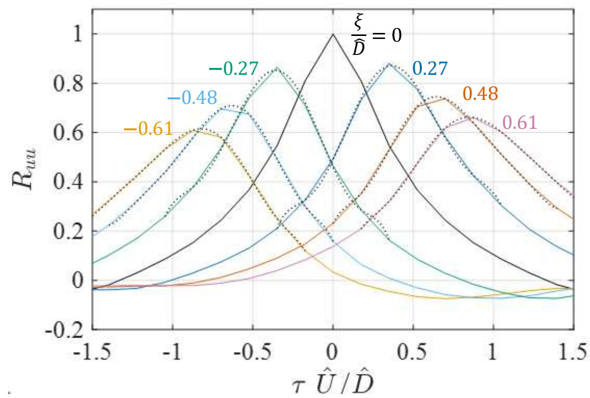

FIG. 4. Space-time correlation R_{uu} on the OSPS at $x/\widehat{D} = 4$ for jet AXI04U. Dashed lines indicate fits by seventh-order polynomials to accurately detect the peak of each correlation.

IV. MEAN FLOW FIELDS

A. Mean axial velocity

Figures 5 and 6 plot isocontours of the normalized mean axial velocity, $\overline{u}/\widehat{U}$, on the plane of symmetry of jets AXI04U and ECC09U, respectively, and compare the RANS and LES solutions. The LES and RANS flow fields are similar, with the LES predicting slightly faster spreading and thus moderately shorter primary potential cores. It is also noted that the wake from the plug is accentuated in the RANS solutions. For jet ECC09U, the asymmetry produced by the eccentricity of the nozzle is evident: there is a significant concentration of low-speed flow on the underside of the primary jet. The lack of tertiary flow on the upper side of ECC09U results in faster growth of the upper portion of the shear layer, thus the potential core for ECC09U is slightly shorter than for AXI04U. We define the length of the primary potential core L_p as the distance from the exit of the primary nozzle (located at $x/\widehat{D} = -1.54$) to the point where the maximum mean axial velocity equals $0.9U_p$. For jet AXI04U, LES gives $L_p/\widehat{D} = 4.5$ and RANS gives $L_p/\widehat{D} = 6.5$. For jet ECC09U, the corresponding values are $L_p/\widehat{D} = 4.2$ and 6.3. As has been noted in previous studies[42,43], the RANS solution has the tendency to over-predict the length of the potential core. Despite this limitation, RANS-based noise predictions can provide useful guidance for the design of quiet propulsion systems[43].

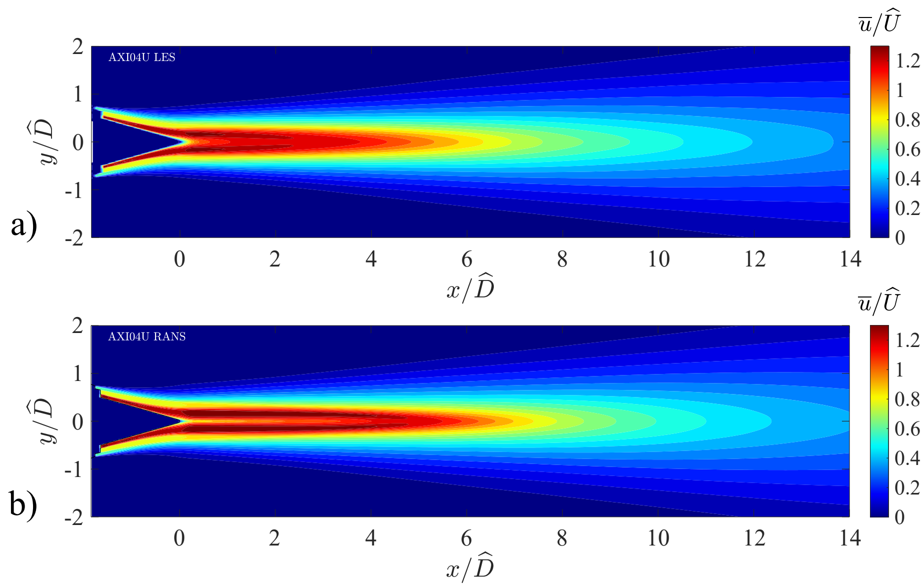

FIG. 5. Isocontours of normalized normalized mean axial velocity $\overline{u}/\widehat{U}$ on the symmetry plane of jet AXI04U. (a) LES and (b) RANS.

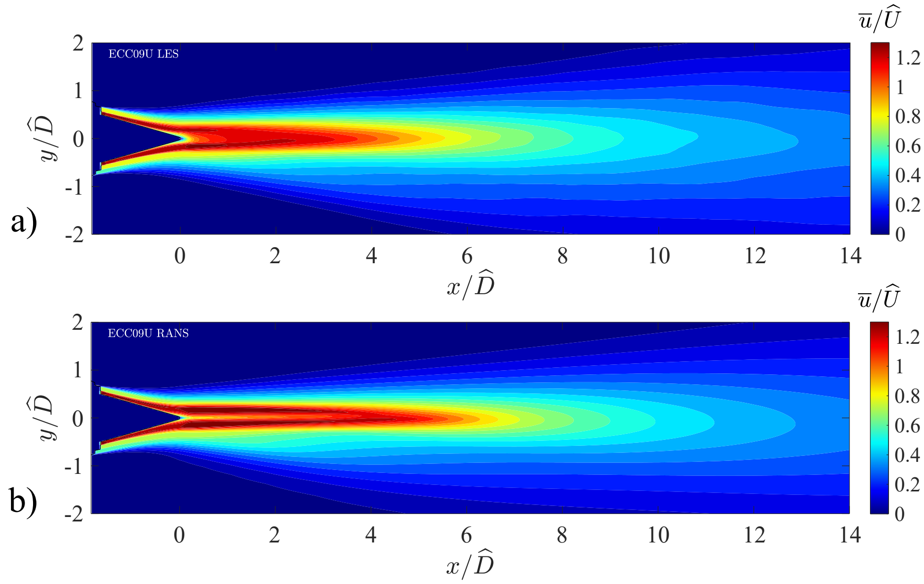

FIG. 6. Isocontours of normalized normalized mean axial velocity $\overline{u}/\widehat{U}$ on the symmetry plane of jet ECC09U. (a) LES and (b) RANS.

B. Reynolds stress

We examine distributions of the magnitude of the principal component of the Reynolds stress tensor

$$g \;=\; |\overline{u'q'}| \tag{3}$$

where u' is the axial velocity fluctuation and q' is the transverse velocity fluctuation in the direction of the mean velocity gradient. For the LES, g is calculated directly from the time-resolved data. For RANS, it is modeled as

$$g \;= \nu_T |\nabla \overline{u}| \tag{4}$$

where ν_T is the turbulent viscosity and $\nabla \overline{u}$ is the gradient of the the mean velocity. For the remainder of the report, g will be loosely referred to as the "Reynolds stress". Physically,

g is a measure of momentum transport by turbulence and represents a direct effect of the coherent turbulence eddies[9]. Therefore, the areas of high Reynolds stress may provide valuable information towards the modeling of the effects of those eddies.

Figure 7 plot isocontours of normalized Reynolds stress $g/\widehat{U}^2$ for jet AXI04U as predicted by LES and RANS. Distinct primary, secondary, and tertiary shear layers are evident near the nozzle exit. As noted in the discussion of the mean velocity profiles, the LES predicts moderately faster mixing rates. Consequently, the merging of the outer shear layers with the inner shear layer is complete by approximately $x/\widehat{D} = 2$ for LES and $x/\widehat{D} = 3$ for RANS. The peak Reynolds stress occurs downstream of this merging. For the LES solution, the peak value of $g/\widehat{U}^2 = 0.010$ occurs at $x/\widehat{D} = 4.4$; for the RANS solution, the peak value of $g/\widehat{U}^2 = 0.012$ occurs at $x/\widehat{D} = 5.0$. Overall, the comparison between RANS and LES is satisfactory both in terms of levels and shapes of the distributions.

The analogous plot of Reynolds stress for jet ECC09U is shown in Fig. 8. The non-smoothness of the LES distribution is due to the limited number of time steps of the solution. On the underside of the jet, the thicker tertiary flow slows down the spreading of the primary shear layer and results in a large suppression of the Reynolds stress. Importantly, the peak Reynolds stress shifts to a lower-speed region, compared to AXI04U, meaning that the most energetic eddies in contact with the ambient have slower convection speed. On the upper side, where there is no tertiary stream, the level of the Reynolds stress is slightly higher than in AXI04U. As for the axisymmetric case, the LES predicts moderately faster mixing rates than does RANS.

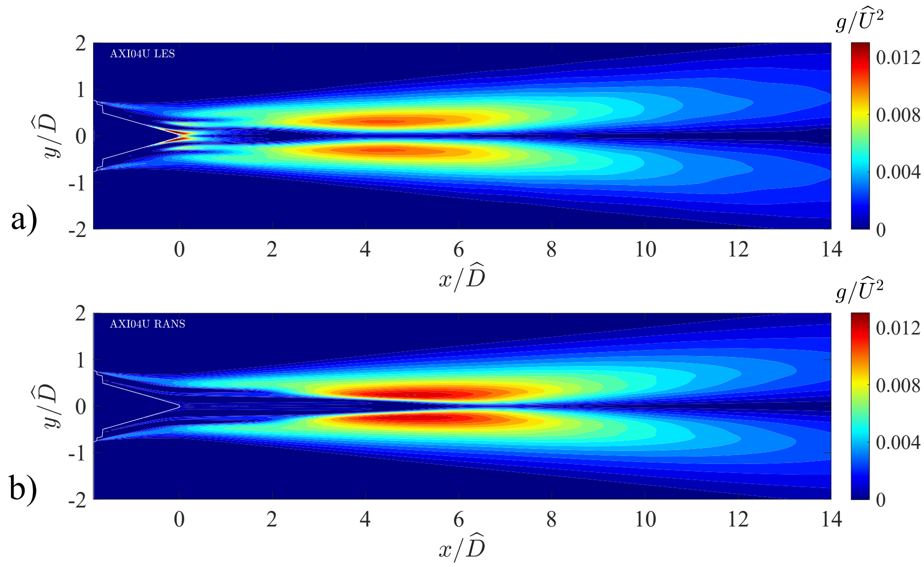

FIG. 7. Isocontours of normalized Reynolds stress $g/\widehat{U}^2$ on a symmetry plane of jet AXI04U. (a) LES and (b) RANS.

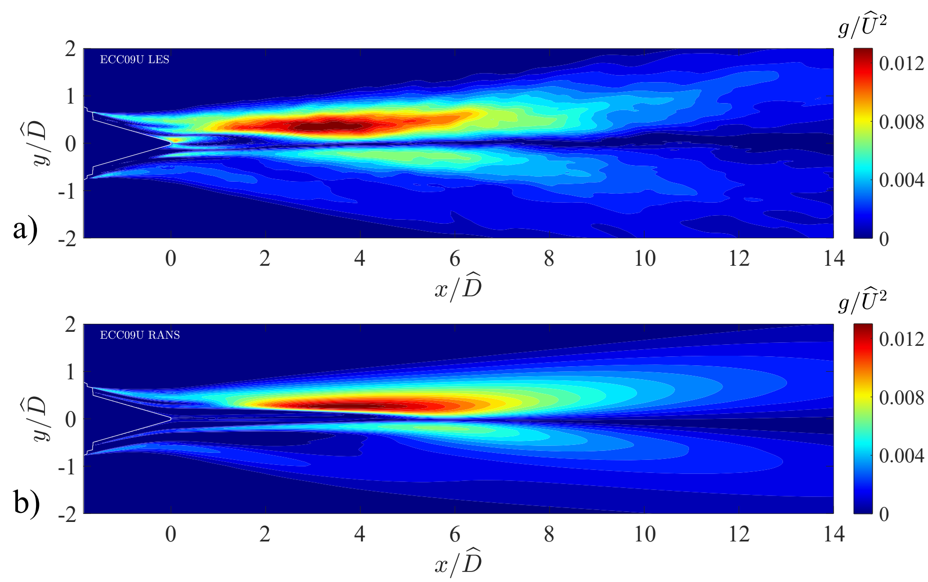

FIG. 8. Isocontours of normalized Reynolds stress $g/\widehat{U}^2$ on the symmetry plane of jet ECC09U. (a) LES and (b) RANS.

V. OUTER SURFACE OF PEAK STRESS

In the acoustic analogy model of Ref. 9 it was surmised that, in multi-stream jets with velocity ratios of relevance to aeroengines, the turbulent eddies in direct contact with the ambient air are the principal noise generators. In a three-stream jet these eddies are initially in the tertiary (outer) shear layer, then progressively transition to the secondary and primary shear layers as the tertiary and secondary flows become mixed with the primary flow (Fig. 1). In the context of RANS, the action of those eddies is represented by the statistics on the outer-most peak of the Reynolds stress g, that is, the first peak of g as one approaches the jet radially from the outside towards the centerline. This results in the concept of the "outer surface of peak stress" (OSPS), which is thought to be important in the understanding and modeling of multi-stream jet noise. Among the most important properties of the eddies in contact with the ambient is their convective velocity U_c and convective Mach number $M_c = U_c/a_\infty$, where a_∞ is the ambient speed of sound. The convective Mach number governs the efficiency with which the eddies radiate sound to the far field; it is thus of paramount significance in the modeling.

The procedure for the detection of the OSPS is a modification of that described in Ref. 9. At a given axial location, the OSPS is detected by constructing rays along the direction of the mean velocity gradient that propagate from the ambient towards the center of the jet; the first (outermost) maximum of the Reynolds stress g along each ray marks the location of the OSPS. This procedure is common for the RANS flow field and the time-averaged LES flow field. Figure 9 offers an example for jet ECC09U based on the RANS solution. The rays start from the low speed region of the jet and propagate inward. They terminate at the first maximum of g, thus defining the OSPS at that particular cross plane. The inner peak of the Reynolds stress is also visible in the figure.

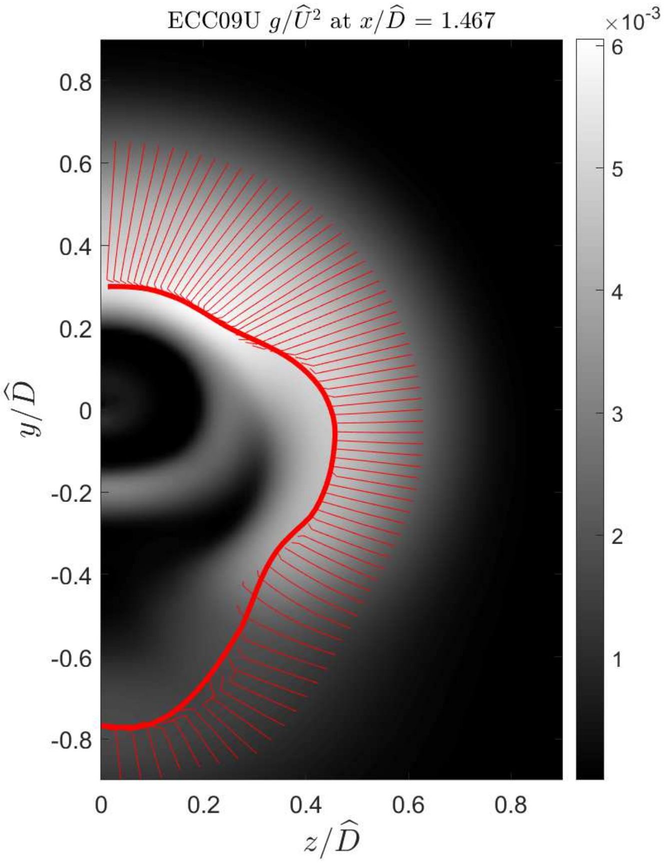

FIG. 9. Detection of outer surface of peak stress (OSPS) at $x/\widehat{D} = 1.467$ for jet ECC09U. Contours indicate the distribution of Reynolds stress on this cross-stream plane. Thin red lines: rays along the mean velocity gradient. Thick red line: OSPS

For the RANS flow field, once the OSPS has been detected, the convective velocity is modeled as the mean axial velocity on the OSPS. Denoting the radius of the OSPS as

$r_{\text{OSPS}}(x,\phi)$, the convective velocity is expressed as

$$U_c(x,\phi) \ = \ \overline{u}\big(x, r_{\text{OSPS}}(x,\phi),\phi\big) \tag{5}$$

For the LES flow field, the convective velocity is determined directly by the space-time correlation of Eq. 2, as explained in the discussion of this equation. An example was shown in Fig. 4.

Three-dimensional views of the the RANS- and LES-derived OSPS for the jets of this study are shown in Figs. 10 and 11, respectively. Color contours indicate the distribution of the convective Mach number M_c on the surfaces. It is evident that LES and RANS produce similar surfaces, with moderate variations in geometry and levels of M_c. The LES surface for ECC09U is jagged due to the limited number of time steps (the corresponding surface for AXI04U appears smoother because it is averaged azimuthally). We discuss general trends evident in both types of solutions; specific differences will be covered in the following subsection. The OSPS of jet AXI04U shows a subtle convergence where the tertiary shear layer becomes mixed with the secondary shear layer, followed by a more pronounced convergence where the outer streams become totally mixed with the primary shear. This sudden collapse is followed by a gradual convergence near the end of the primary potential core, downstream of which the OSPS diverges slowly. The peak M_c occurs shortly downstream of the depletion of the outer streams. The asymmetry of nozzle ECC09U has a strong effect on the shape of its OSPS. The convergence from tertiary to secondary shear layer, as well as the stronger collapse on the primary layer, have a clear dependence on the azimuthal angle ϕ. Those transition points move downstream as ϕ tends to 0, the downward direction. In addition, in the proximity of $\phi = 0°$, the tertiary shear layer interacts minimally with the secondary and primary layers: it diverges until it vanishes due to spreading. At that point, it stops representing the outer peak of Reynolds stress and the OSPS collapses on the primary shear layer. This creates the "bulge" visible in the downwards direction of Figs. 10(b) and 11(b). Overall, the outward deflection of the OSPS on the underside of the jet causes a large reduction in convective Mach M_c. This is key to the noise reduction induced by nozzle ECC09U in the downward direction, as seen in Fig. 3.

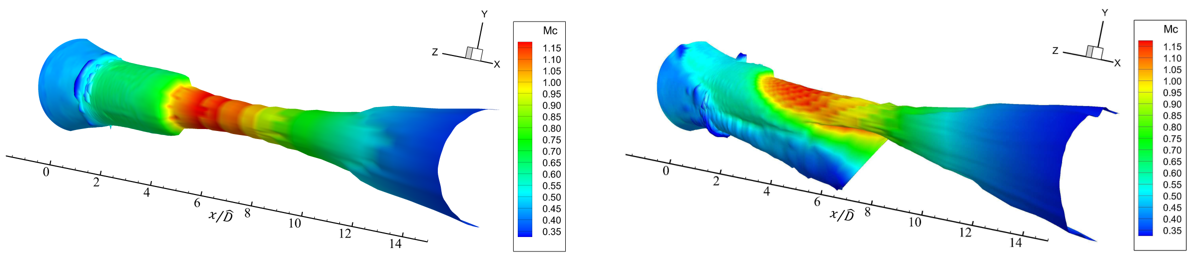

(a) Jet AXI04U

(b) Jet ECC09U

FIG. 10. RANS-based OSPS with contours of convective Mach number M_c.

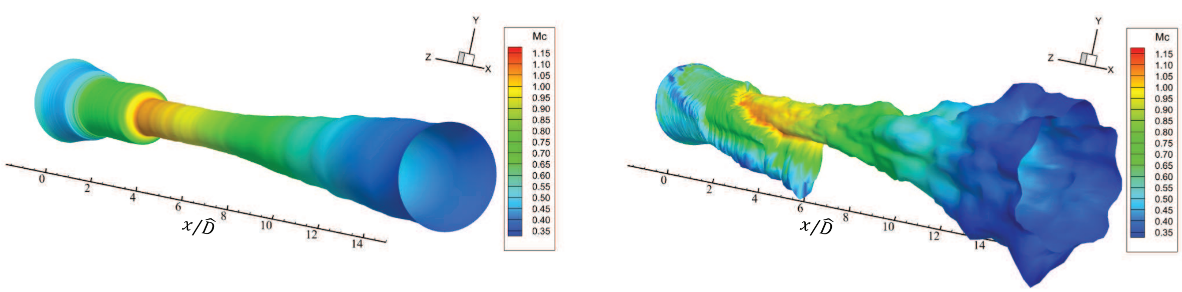

(a) Jet AXI04U

(b) Jet ECC09U

FIG. 11. LES-based OSPS with contours of convective Mach number M_c.

A. Comparisons of LES and RANS results

Having discussed the detection and broad features of the OSPS, we proceed with detailed comparisons of the geometries and convective velocity distributions obtained by the RANS and LES solutions for the OSPS of jets AXI04U and ECC09U.

1. Jet AXI04U

Figure 12(a) plots the radial coordinates of the OSPS of jet AXI04U as computed by RANS and LES. The two predictions are practically identical up to $x/\widehat{D} = 1.7$, with the plot showing clearly the inward transition of the OSPS from the tertiary to the secondary, and then to the primary shear layer. This transition occurs in LES about 0.8 diameters upstream than in RANS. For $x/\widehat{D} > 1.7$, the two surfaces are close but the LES result is shifted outward, reflecting the faster spreading of the LES jet.

The comparison of convective velocities on the OSPS is seen in Fig. 12(b). The RANS- and LES-based trends are similar and show an increase in U_c as the most energetic eddies move from the tertiary (low speed) to the secondary (medium speed), and then to the primary (high speed) shear layer. At this point the convective velocity peaks and starts to decline, following the decay of the mean velocity past the end of the potential core. Those three initial velocity levels are approximately $0.36\widehat{U}$, $0.55\widehat{U}$, and $0.82\widehat{U}$ and correspond to $0.56U_t$, $0.64U_s$, and $0.60U_p$ respectively, which are close to the typical value of $0.6U_j$ in the case of single-stream jets[15]. There are moderate quantitative differences between the RANS and LES results, with RANS predicting a peak value of U_c that is about 14% higher than that predicted by LES. These peaks of U_c also take place at slightly different locations, $x/\widehat{D} = 3.6$ for RANS and $x/\widehat{D} = 2.0$ for LES, which is explained by the difference in transition to the primary stream in each OSPS.

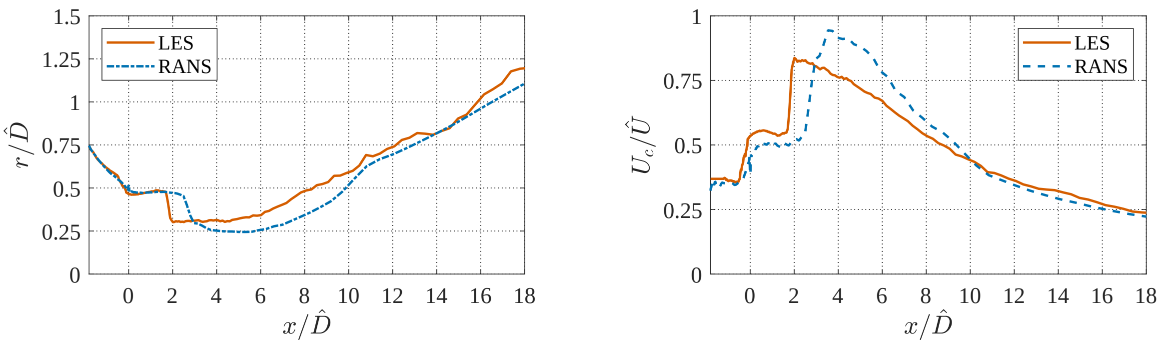

(a) Radial coordinate of OSPS.

(b) U_c distribution on the OSPS.

FIG. 12. RANS and LES results regarding the OSPS of jet AXI04U.

2. Jet ECC09U

Because of the eccentricity of nozzle ECC09U, the resulting OSPS shape is dependent on the azimuthal angle ϕ. For brevity we only show comparisons for $\phi = 0°$ and $\phi = 180°$. The radial coordinate results for $\phi = 0°$ are plotted in Fig. 13(a). There is reasonable agreement between the RANS and LES predictions, both capturing the collapse of the OSPS near $x/\widehat{D} = 4.3$, where the outer shear layer vanishes and the OSPS transitions to the primary shear layer. The axial location of this transition is earlier in the LES than in the RANS solution, consistent with the faster spreading of the LES flow, also seen for jet AXI04U. Downstream of this transition the curves have similar trends, with the LES-based OSPS showing a faster spreading and therefore an outward shift. Past $x/\widehat{D} = 13$ the LES-based

OSPS loses accuracy due to the lack of convergence of the statistics. Figure 13(b) compares convective velocities obtained by modeling on RANS and two-point correlations on LES. The noise on the LES-based U_c at $x/\widehat{D} < -1$ is not considered physical but a result of the numerical difficulty in locating the OSPS and performing two-point correlations very close to the tertiary nozzle lip. Overall, the LES and RANS curves are similar and show a slightly decaying U_c where the OSPS occurs on the outer shear layer. Near $x/\widehat{D} = 4.3$, the collapse of the OSPS to the primary shear layer causes the convective velocity to rise suddenly. The LES predicts a peak U_c value about 9% lower than that obtained from the RANS solution.

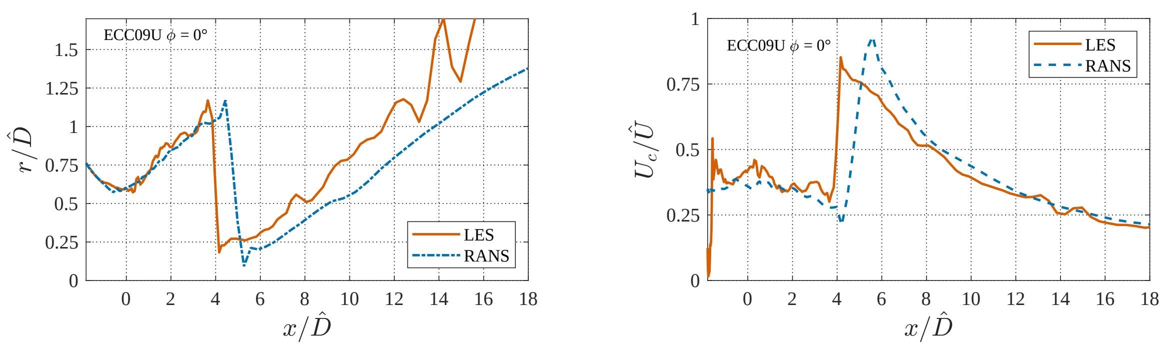

(a) Radial distribution of OSPS.

(b) U_c distribution on the OSPS.

FIG. 13. RANS and LES results regarding the OSPS of jet ECC09U on $\phi = 0°$.

Corresponding results for $\phi = 180°$ are shown in Fig. 14. The radial coordinates show similar trends, with an overall faster spreading of the LES jet. Because the tertiary stream is deflected away from the top of the nozzle, the OSPS follows the secondary shear layer, which is quickly merged with the primary shear layer. This transition occurs near $x/\widehat{D} = 0.7$ for LES and around $x/\widehat{D} = 1.2$ for RANS. Downstream of this transition, the LES result shows a more rapid spreading rate. Despite the location discrepancy seen in Fig. 14(a), the RANS- and LES-based convective velocities plotted in Fig. 14(b) are still in overall agreement. Similarly to jet AXI04U, there is a stepped increment in the convective velocity as the shear layers mix. In this case, because the tertiary flow is deflected such that there are only primary and secondary flows at the top of the jet, only one sudden rise is seen. The fact that LES predicts the transition from secondary to primary shear layer upstream from RANS naturally leads to an earlier rise of the corresponding convective velocity. After that, the lower LES-based U_c is explained by the faster spreading of the OSPS.

Comparing the U_c distribution on the underside of jet ECC09U (Fig. 13(b)) with that of jet AXI04U (Fig. 12(b)) we note a substantial reduction in the region $0 \leq x/\widehat{D} \leq 4$. This region influences the middle and high frequencies, which are of particular relevance to aircraft noise. The peak convective Mach number in that region is reduced from 1.10 to 0.57 in the LES solution; and 1.19 to 0.48 in the RANS solution. This reduction occurs because the outer-most eddies are shifted to a lower velocity regime. The resulting decrease in radiation efficiency is evident by the large reduction in sound pressure level seen in Fig. 3 at the mid and high frequencies. Even though there are discrepancies on the order of 10% between RANS and LES in the prediction of U_c, RANS captures well the changes in M_c, and their spatial extent, and is thus expected to provide useful guidance in a differential noise prediction model.

VI. RADIATOR SURFACE

The radiator surface is a surface close to the jet axis on and outside of which the propagation of pressure perturbation is governed by the homogeneous linear wave equation. It is

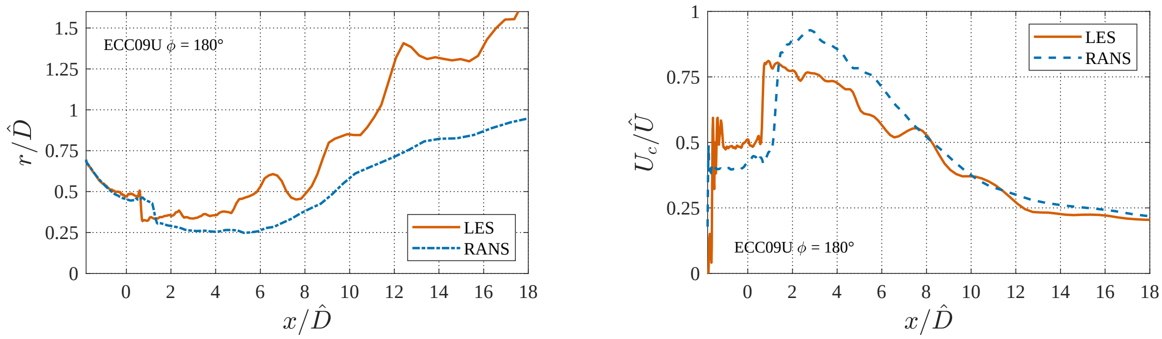

(a) Radial distribution of OSPS

(b) U_c distribution on the OSPS

FIG. 14. RANS and LES results regarding the OSPS of jet ECC09U on $\phi = 180°$.

on this surface that the noise sources could be modeled in the form of linear partial fields[25]. This model would be informed by turbulence statistics of the vortical field computed by RANS. As we move away from this surface, the hydrodynamic information is lost rapidly. One of the most important elements of a surface-based source model is the convective velocity U_c. This section provides a specific definition for the radiator surface, evaluates it for the jets of this study, and offers a practical criterion for locating it based on the RANS solution.

A. Definition

It is desirable that the convective velocity distribution on the radiator surface matches that of the underlying eddies that dominate noise emission. It is then sensible to look for a connection between the convective velocity distributions on the OSPS and at the edge of the jet. The first issue to address is whether the LES-based convective velocity should be based on space-time correlations of the axial velocity fluctuation u' or the pressure fluctuation

p'. Due to their physical associations, we designate u'-based space-time correlations for the inner vortical field, where the turbulent structures affect the velocity of the flow directly; and p'-based correlations for the region near and beyond the the edge of the jet, where we seek the pressure imprint of the vortical eddies. This choice is supported by earlier works, which found that space-time correlations of u' capture the extent of the turbulence eddies but lose their effects (their "footprint") away from them. On the other hand, correlations based on p' capture better the footprint of the turbulence events and thus show a physically meaningful transition from hydrodynamic to acoustic fields[44]. Accordingly, the specific definition of the radiator used in the present work is the surface near the edge of the jet where the R_{pp}-based U_c matches the R_{uu}-based convective velocity on the OSPS at the same axial and azimuthal locations.

B. Evaluation for the jets of this study

Figure 15 displays isocontours of R_{pp}-based U_c, normalized by the equivalent velocity $\widehat{U}$, on the meridional planes of jet AXI04U and jet ECC09U at ϕ=0° and ϕ=180°. The result for AXI04U has been averaged in the azimuthal direction. At a given axial location, U_c has a radial trend whereby it decreases outside the OSPS, reaches a minimum, then rises sharply. The sharp rise is associated with the transition from the hydrodynamic to the acoustic fields. Previous studies have shown similar trends for single- and multi-stream jets[15,16,45]. To achieve the aforementioned property of the radiator surface, we search for a surface near the edge of the jet where the U_c distribution matches that on the OSPS. The result are the white lines plotted in Fig. 15. They track very closely the hydrodynamic-acoustic

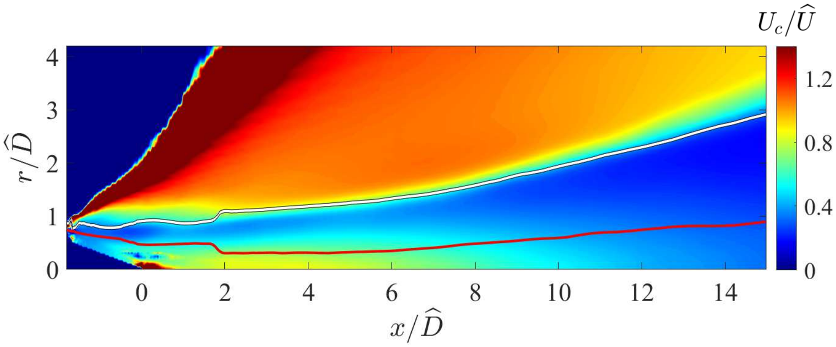

(a) Jet AXI04U.

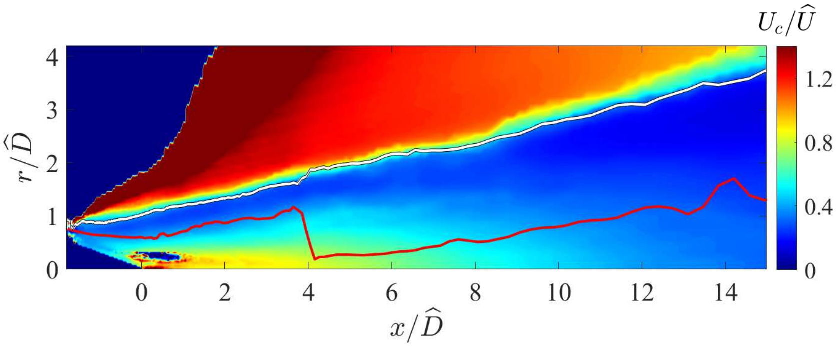

(b) Jet ECC09U at $\phi = 0°$.

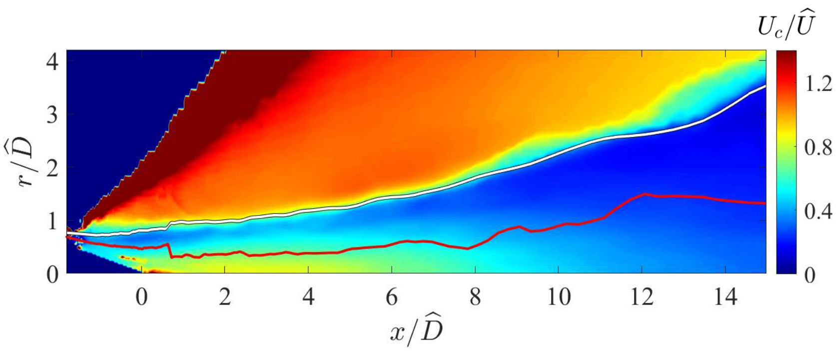

(c) Jet ECC09U at $\phi = 180°$.

FIG. 15. Distribution of normalized convective velocity $U_c/\widehat{U}$ as determined by space-time correlations based on p' on meridional planes of jets AXI04U and ECC09U. White lines: radiator surface; red lines: OSPS based on LES.

transition of the U_c maps. The smoothness of the U_c-match lines, and their proximity to the hydrodynamic/acoustic boundary in the R_{pp}-based U_c, suggest that the U_c information on the OSPS is transmitted to the jet rotational/irrotational boundary. It is in fact quite remarkable that a highly distorted OSPS, such as that of jet ECC09U, yields a smooth radiator surface. This is even more apparent in the three-dimensional renderings of Fig. 16 which overlays the LES-derived OSPS with the radiator surface for jets AXI04U and ECC09U. The results provide encouragement that there is a surface, having the desired properties of the radiator surface, on which the RANS-derived convective velocity (on the OSPS) would inform the definition of the partial fields for noise source modeling.

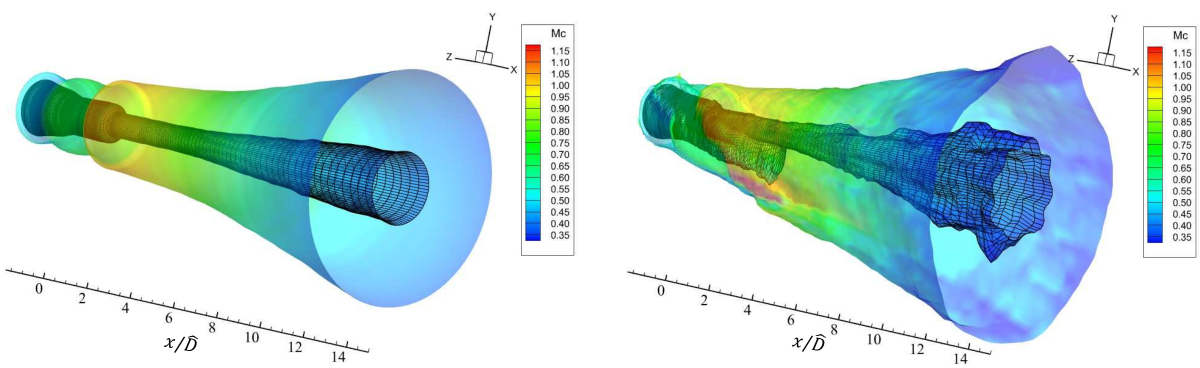

(a) Jet AXI04U

(b) Jet ECC09U

FIG. 16. Radiator surfaces and LES-based OSPS with contours of convective Mach number M_c.

It is instructive to examine the effect of the eccentricity of the tertiary stream on the pressure distribution on the radiator surface. To this end, Fig. 17 plots the axial distribution of the root mean square of p', $p'_{\rm rms}$, on the radiator surfaces of jets AXI04U and ECC09U at $\phi = 0°$ (downward direction). The eccentricity reduces the pressure level by factor of about two, which is consistent with the reduction in Reynolds stress seen when comparing Figs. 7(a) and 8(a). This reduction, and the decline in radiation efficiency due to the lower convective Mach number, are factors that contribute to the reduction in far-field sound pressure level seen in Fig. 3.

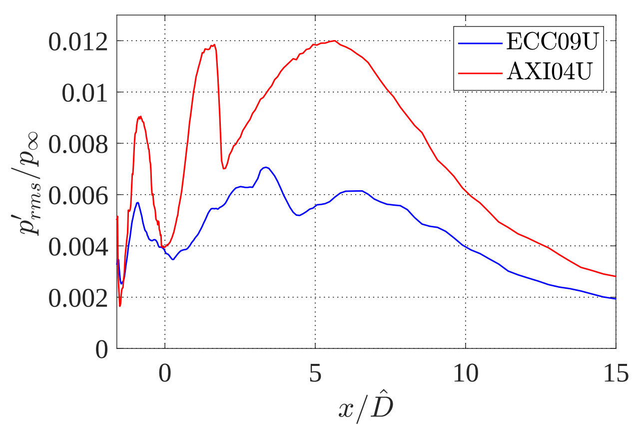

FIG. 17. Distribution of p'_{rms}, normalized by the ambient pressure p_∞, on the radiator surfaces of jets AXI04U and ECC09U at $\phi = 0°$.

C. Approximation based on mean flow

A predictive approach based on RANS alone would not have the benefit of the space-time correlations to locate the radiator surface. We thus search for a criterion based on the mean flow field that would yield an approximate representation of the radiator surface. The main attribute of the radiator surface is that it is placed at the boundary between the rotational and irrotational fields. It is therefore relevant to study the mean vorticity distribution as a means of developing the desired criterion. Figure 18 plots isocontours of normalized mean vorticity magnitude $|\boldsymbol{\varpi}|\widehat{D}/\widehat{U}$ on the meridional plane of jet AXI04U. The magnitude has a wide dynamic range and reaches peak values of approximately $|\boldsymbol{\varpi}|\widehat{D}/\widehat{U} = 20$ in the shear layers near the nozzle exit. To accentuate the vorticity distribution near the jet edge, a smaller dynamic range has been applied so that the core vortical region appears saturated. The radiator surface is included in Fig. 18. It is observed that the radiator surface follows the outer edge of the mean vorticity field. The same observation holds for jet ECC09U and is not shown here for brevity.

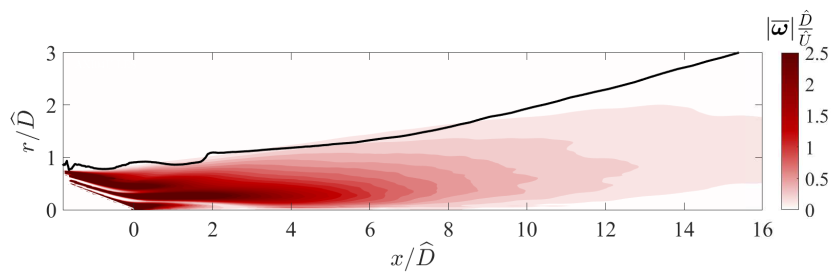

FIG. 18. Isocontours of normalized magnitude of mean vorticity $|\overline{\boldsymbol{\omega}}|\widehat{D}/\widehat{U}$ on jet AXI04U. Black line: radiator surface based on U_c-match criterion.

While a fixed threshold of $|\overline{\boldsymbol{\omega}}|\widehat{D}/\widehat{U}$ may work well around the potential core of the jet, it will fail downstream as the magnitude of the mean vorticity decays together with the maximum mean velocity of the jet. To account for this, we consider a criterion based on the local mean vorticity. Specifically, we seek the surface defined by

$$|\overline{\boldsymbol{\omega}}|(x,r,\phi) \;=\; \kappa|\overline{\boldsymbol{\omega}}|_{\,\mathrm{om}}(x,\phi)\;, \quad r \geq r_{\,\mathrm{om}}(x,\phi) \tag{6}$$

where $|\overline{\boldsymbol{\omega}}|_{\,\mathrm{om}}$ is the outermost maximum of $|\overline{\boldsymbol{\omega}}|$ at a given axial and azimuthal location, $r_{\,\mathrm{om}}$ is the radial location of this maximum, and $\kappa < 1$ is a threshold. The search procedure for $|\overline{\boldsymbol{\omega}}|_{\,\mathrm{om}}$ is similar to the detection of the OSPS exemplified in Fig. 9. Then, as Eq. 6 indicates, the threshold is applied as one approaches the jet from the ambient towards the centerline.

It was found that the threshold $\kappa = 0.125$ works satisfactorily for both jets of this study, as illustrated in Figs. 19 and 20. The figures demonstrate an excellent representation of the radiator surface using the criterion of Eq. 6. Even though this is based on only two jets, it builds confidence that a RANS-based criterion for locating the radiator surface is achievable.

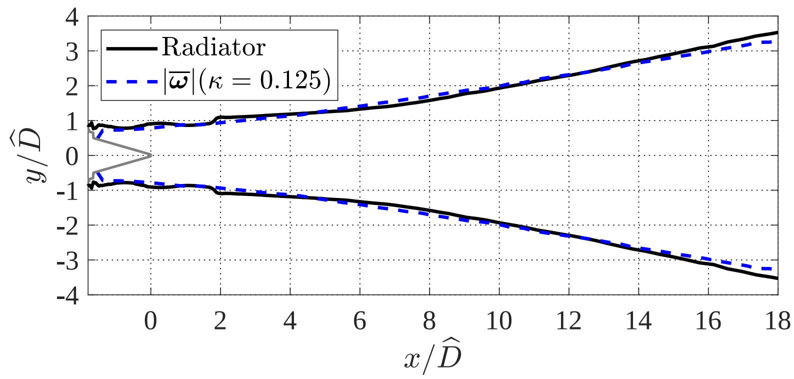

(a) Jet AXI04U.

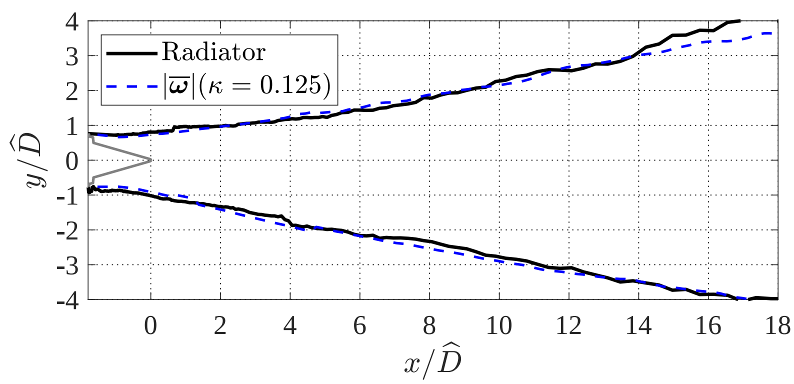

(b) Jet ECC09U.

FIG. 19. Comparison of radiator surface (black solid lines) with surface based on the mean vorticity criterion of Eq. 6 (dashed blue lines) on symmetry planes of jets (a) AXI04U and (b) ECC09U.

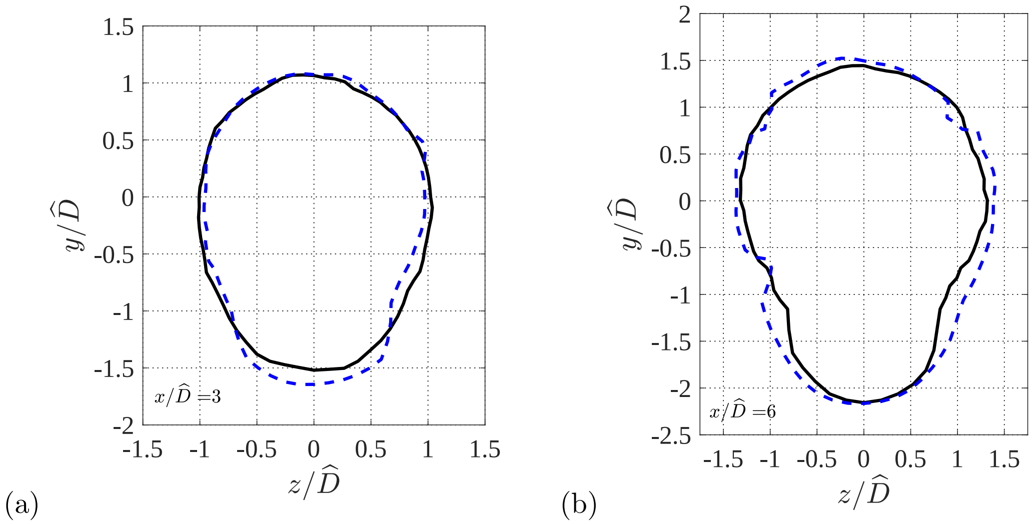

FIG. 20. Comparison of radiator surface (black solid lines) with surfaces based on mean vorticity of Eq. 6 (dashed blue lines) on cross-sectional planes of jet ECC09U: (a) $x/\widehat{D} = 3$; (b) $x/\widehat{D} = 6$.

VII. 2D SPACE-TIME CORRELATIONS

The connection between the inner vortical field and the edge of the jet is further investigated using two-dimensional space-time correlations of the LES data. The focus is on the interaction between turbulent eddies near the inner (high-speed) shear layer and the rest of the domain, with emphasis on events near the radiator surface. For the reasons given in Section VI, we consider the correlation R_{up} between u' in the high-speed turbulent region and p' elsewhere. The formulation of Eq. 2 is used with reference point $\mathbf{x}_0 = (x_0, r_0, 0)$ and displaced point $\mathbf{x} = (x, r, 0)$.

On the meridional plane $\phi = 0°$, the reference point is placed at $(x_0, r_0) = (2.0, 0.3)\widehat{D}$. This point is on the OSPS of jet AXI04U and near the middle of the high-speed shear layer of jet ECC09U. The resulting space-time correlation $\widehat{R}_{up}$ is plotted in Fig. 21 for jets

AXI04U and ECC09U at three time separations. The evolution of $\widehat{R}_{up}$ for AXI04U shows two main lobes of opposite signs traveling downstream at a speed slightly faster than $0.6\widehat{U}$. At zero time separation (τ=0), the lobes show a strong correlation pattern radiating from the vortical region to the radiator surface and then on to the near acoustic field. For non-zero time separations ($\tau = \pm 1.92\widehat{D}/\widehat{U}$), the correlations remain strong in the near acoustic field but weaken inside the vortical region. The correlation peaks near the radiator surface represent the footprint of large turbulent structures that pass through the reference point and dominate the surrounding linear field[46]. However, inside the vortical field those large eddies coexist with smaller scales that become uncorrelated quickly and thus decrease the values of two-point correlations for $\tau \neq 0$. The fact that the peaks of correlation linked to the linear field follow well the location of the radiator surface is further confirmation of its appropriate placement in Section VI.

In comparison with jet AXI04U, jet ECC09U shows much lower values of correlations at all time separations. At zero time separation, the peak correlation of ECC09U in the near acoustic field is $R_{up} = -0.13$ versus $R_{up} = -0.21$ for AXI04U. At non-zero time separation, the correlations for ECC09U become even weaker. The thickened low-speed flow of jet ECC09U not only suppresses the turbulence level of the inner shear layer, as evidenced in Fig. 8, but also weakens the correlation between the inner shear layer and the emitted acoustic field. The reduced correlation can be attributed to the lower radiation efficiency of the eddies in the inner shear layer.

Movies of the time evolution of the 2D space-time correlations in Fig. 21 are available in supplementary files SuppPubmm1.avi and SuppPubmm1.avi for jets AXI04U and ECC09U,

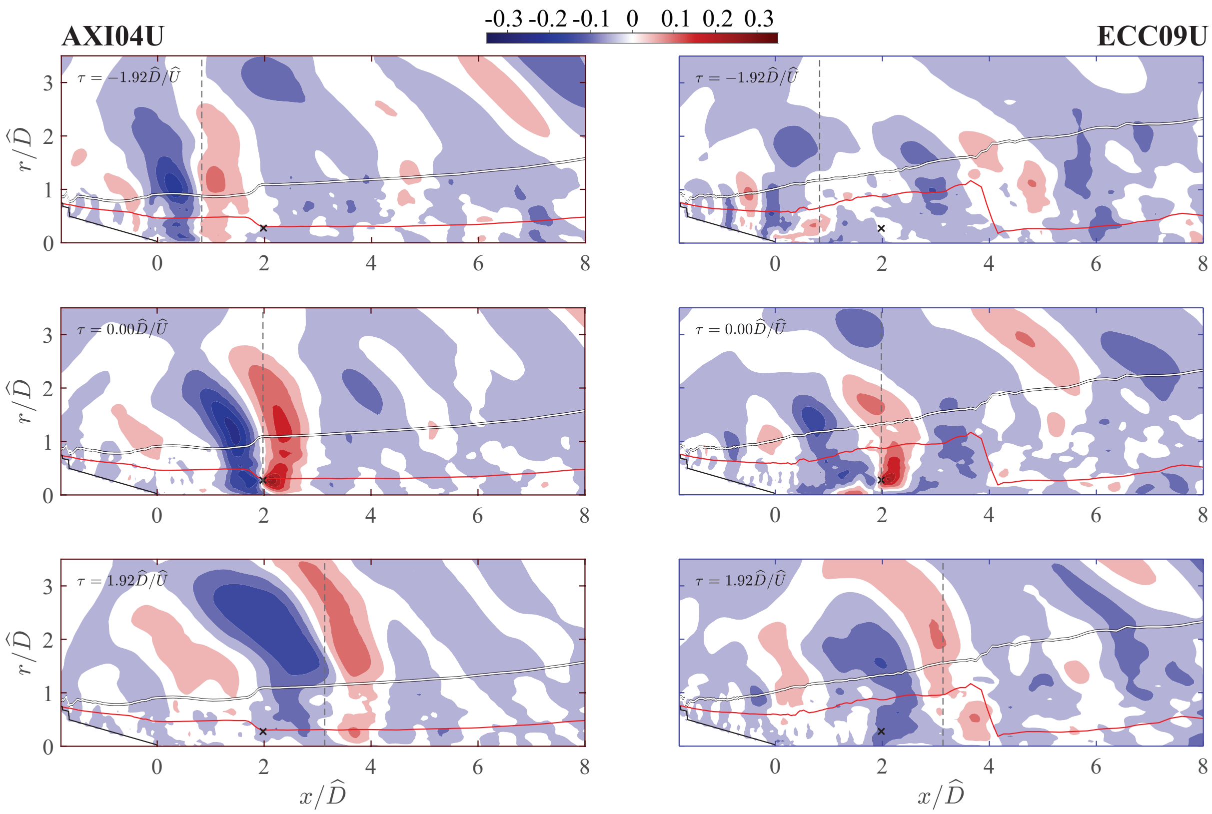

FIG. 21. Contours of R_{up} with reference point $(x_0, r_0) = (2, 0.3)\widehat{D}$ for jets AXI04U (left column) and ECC09U (right column) at azimuthal angle $\phi = 0°$. Time separations: $\tau = -1.92\widehat{D}/\widehat{U}$ (top row), $\tau = 0$ (middle row), and $\tau = 1.92\widehat{D}/\widehat{U}$ (bottom row). Red line: SPS. White line: radiator surface. Black dashed vertical line: positions for a downstream convection at velocity $0.6\widehat{U}$.

respectively. The movies enable a more complete view of the trends discussed above regarding the correlations and their suppression (See supplementary material at [URL] for the 2D space-time correlation movies.)

VIII. CONCLUDING REMARKS

This computational study explored connections between the vortical and near-acoustic fields of multi-stream jets whose understanding will aid in the noise source modeling of these complex flows. The ultimate goal is development of linear, surface-based models that would be informed by low-cost RANS solutions. The study used two triple-stream jets, one coaxial and the other with eccentric tertiary flow that yields noise suppression in preferred directions. The jets exhausted at conditions simulating the takeoff set point of a supersonic turbofan engine. An essential requirement for the model is accurate representation of the convective velocity U_c of the noise-generating turbulent eddies.

Large Eddy Simulations were used to assess key assumptions in the RANS-based model. Direct evaluation of the Reynolds stress and convective velocity U_c from the LES show reasonable agreement with the RANS-based modeled values. This suggests the validity of modeling the convective velocity of the noise-generating turbulent as the mean axial velocity on the outer surface of peak stress (OSPS). The LES results also help define a "radiator surface" on which the jet noise source model would be prescribed. The radiator surface is located at the boundary between the rotational and irrotational field and is defined as the surface near the jet edge on which the U_c distribution, obtained from space-time correlations of pressure fluctuations, matches the convective velocity based on axial velocity fluctuations on the OSPS. A criterion based on the mean vorticity is formulated that accurately approximates the shape of this surface. The connection between the inner vortical field and the edge of the jet is also investigated through two-dimensional space-time correlations of the velocity and pressure fields. The correlations shed light on the noise generation from the high-speed region of the jet and show how the asymmetry of the tertiary stream, and the resulting thicker low-speed flow, weakens the radiation efficiency of the high-speed eddies.

One of the most important finding of this study is that there is a surface in the linear near field of a complex multistream jet, the radiator surface, on which pressure disturbances convect at the same speed as the vortical eddies that are considered to be the main noise generators. This convective speed can be modeled as the mean flow velocity on the OSPS, therefore can be informed by a RANS solution. Nozzle asymmetry causes changes in the geometry of the OSPS and convective velocity that are captured by RANS with a reasonable degree of accuracy. Despite the irregular shape of the OSPS, the radiator surface is relatively smooth and its geometry can be approximated using a mean-vorticity criterion, therefore it can also be based on the RANS solution. We conclude that RANS shows promise in predicting two of the most important elements in the proposed modeling – the geometry of the radiator surface and the convective velocity distribution on it. A complete model will require additional information including length and time scales. It is hoped that these can also be based on RANS, and this is the topic of current work.

ACKNOWLEDGMENT

This work was partially funded by NASA Phase II SBIR contract 80NSSC19C0089, under technical monitor Dr. Brenda Henderson. Spectral Energies, LLC was the prime contractor. A.A. has also received support from a Balsells Fellowship.

REFERENCES

[1]G. Brès, F. Ham, J. Nichols, and S. Lele, "Unstructured large-eddy simulations of supersonic jets," AIAA Journal **55**(4) (2017) doi: 10.2514/1.J055084.

[2]B. Henderson, "Aeroacoustics of three-stream jets," AIAA Paper 2012-2159 (2012) doi: 10.2514/6.2012-2159.

[3]B. Henderson, S. Leib, and M. Wernet, "Measurements and predictions of the noise from three-stream jets," AIAA Paper 2015-3120 (2015) doi: 10.2514/6.2015-3120.

[4]B. S. Henderson and M. Wernet, "Characterization of three-stream jet flow fields," AIAA Paper 2016-1636 (2016) doi: 10.2514/6.2016-1636.

[5]B. S. Henderson and D. L. Huff, "The aeroacoustics of offset three-stream jets for future commercial supersonic aircraft," AIAA Paper 2016-2992 (2016) doi: 10.2514/6.2016-2992.

[6]D. Papamoschou, V. Phong, J. Xiong, and F. Liu, "Quiet nozzle concepts for three-stream jets," AIAA Paper 2016-0523 (2016) doi: 10.2514/6.2016-0523.

[7]V. Phong and D. Papamoschou, "Investigation of isolated and installed three-stream jets from offset nozzles," AIAA Paper 2017-0005 (2017) doi: 10.2514/6.2017-0005.

[8]S. Leib, "Modeling sound propagation through non-axisymmetric jets," NASA/CR–2014-218107 (2014).

[9]D. Papamoschou, "Modelling of noise reduction in complex multistream jets," Journal of Fluid Mechanics **834**, 555–599 (2018) doi: 10.1017/jfm.2017.730.

[10] J. Tanna and P. Morris, "The noise from normal-velocity-profile coannular jets," Journal of Sound and Vibration **98**(2), 213–234 (1985) doi: 10.1016/0022-460X(85)90386-4.

[11] M. Fisher, G. Preston, and W. Bryce, "A modelling of the noise from simple coaxial jets, Part I: With unheated primary flow," Journal of Sound and Vibration **209**(3), 385–403 (1998) doi: 10.1006/jsvi.1997.1218.

[12] D. Papamoschou and S. Rostamimonjezi, "Effect of velocity ratio on noise source distribution of coaxial jets," AIAA Journal **48**(7), 1504–1512 (2010) doi: 10.2514/1.J050140.

[13] C. Tinney and P. Jordan, "The near pressure field of co-axial subsonic jets," Journal of Fluid Mechanics **611**, 175–204 (2008) doi: 10.1017/S0022112008001833.

[14] D. Papamoschou and V. Phong, "The very near pressure field of single- and multi-stream jets," AIAA Paper 2017-0230 (2017) doi: 10.2514/6.2017-0230.

[15] J. E. Bridges and M. P. Wernet, "Measurements of turbulent convection speeds in multistream jets using time-resolved PIV," AIAA Paper 2017-4041 (2017) doi: 10.2514/6.2017-4041.

[16] M. Stuber, K. T. Lowe, and W. F. Ng, "Synthesis of convection velocity and turbulence measurements in three-stream jets," Experiments in Fluids **60**(5), 83 (2019) doi: 10.1007/s00348-019-2730-5.

[17] C. Prasad and P. Morris, "Steady active control of noise radiation from highly heated supersonic jets," Journal of the Acoustical Society of America **149**(2), 1306–1317 (2021) doi: 10.1121/10.0003570.

[18] K. Daniel, D. Mayo Jr, K. T. Lowe, and W. Ng, "Experimental investigation on the acoustic field and convection velocity of structures in a heated jet with centered thermal non-uniformity," AIAA Paper 2019-1300 (2019) doi: 10.2514/6.2019-1300.

[19] A. Pilon and A. Lyrintzis, "Development of an improved Kirchhoff method for jet aeroacoustics," AIAA Journal **36**(5), 783–790 (1998) doi: 10.2514/2.437.

[20] C. Tam, N. Pastouchenko, and K. Viswanathan, "Extension of the near acoustic field of a jet to the far field," Procedia Engineering **6**, 9–18 (2010) doi: 10.1016/j.proeng.2010.09.002.

[21] D.-C. Mincu, E. Manoha, C. Parzani, J. Chappuis, S. Redonnet, R. Davy, and M. Escouflaire, "Numerical and experimental characterization of aft-fan noise for isolated and installed configurations," AIAA Paper 2010-3918 (2010) doi: 10.2514/6.2010-3918.

[22] P. Morris, "A note on noise generation by large scale turbulent structures in subsonic and supersonic jets," International Journal of Aeroacoustics **8**(4), 301–316 (2009) doi: 10.1260/147547209787548921.

[23] R. Reba, S. Narayanan, and T. Colonius, "Wave-packet models for large-scale mixing noise," International Journal of Aeroacoustics **9**, 533–558 (2010) doi: 10.1260/1475-472X.9.4-5.533.

[24] D. Papamoschou, "Wavepacket modeling of the jet noise source," International Journal of Aeroacoustics **17**(1-2), 52–69 (2018) doi: 10.1177/1475472X17743653.

[25] D. Papamoschou, "On the connection between near and far pressure fields of a turbulent jet," AIAA Paper 2018-1251 (2018) doi: 10.2514/6.2018-1251.

[26]K. Gudmundsson and T. Colonius, "Instability wave models for the near-field fluctuations of turbulent jets," Journal of Fluid Mechanics **689**, 97–128 (2011) doi: 10.1017/jfm.2011.401.

[27]P. Jordan and T. Colonius, "Wave packets and turbulent jet noise," Annual Review of Fluid Mechanics **45**, 173–195 (2013) doi: 10.1146/annurev-fluid-011212-140756.

[28]A. Cavalieri, D. Rodriguez, P. Jordan, T. Colonius, and Y. Gervais, "Wavepackets in the velocity field of turbulent jets," Journal of Fluid Mechanics **730**, 559–592 (2013) doi: 10.1017/jfm.2013.346.

[29]A. Cavalieri, P. Jordan, and L. Lesshafft, "Wave-packet models for jet dynamics and sound radiation," Applied Mechanics Reviews **71**, 020802–1 –27 (2019) doi: 10.1115/1.4042736.

[30]D. Papamoschou, "Prediction of jet noise shielding," AIAA Paper 2010-0653 (2010) doi: 10.2514/6.2010-653.

[31]S. Piantanida, V. Jaunet, J. Huber, W. Wolf, P. Jordan, and A. Cavalieri, "Scattering of turbulent-jet wavepackets by a swept trailing edge," Journal of the Acoustical Society of America **140**(6), 4350–4359 (2016) doi: 10.1121/1.4971425.

[32]C. Ho, "Near field pressure fluctuations in a circular jet," NASA CR-179847 (1985).

[33]K. Zaman, "Flow field and near and far sound field of a subsonic jet," Journal of Sound and Vibration **106**(1), 1–16 (1986) doi: https://doi.org/10.1016/S0022-460X(86)80170-5.

[34]D. Papamoschou and V. Phong, "Perceived noise assessment of offset three-stream nozzles for low noise supersonic aircraft," AIAA Paper 2018-1740 (2018) doi:

10.2514/6.2018-1740.

[35] J. Xiong, P. Nielsen, F. Liu, and D. Papamoschou, "Computation of high-speed coaxial jets with fan flow deflection," AIAA Journal **48**(10), 2249–2262 (2010) doi: 10.2514/1.J050331.

[36] A. Jameson, W. Schmidt, and E. Turkel, "Numerical solutions of the euler equations by finite volume methods using Runge-Kutta time stepping schemes," AIAA Paper 1981-1259 (1981) doi: 10.2514/6.1981-1259.

[37] F. Menter, "Two-equation eddy-viscosity turbulence models for engineering applications," AIAA Journal **32**(8), 1598–1605 (1994) doi: 10.2514/3.12149.

[38] P. L. Roe, "Approximate Riemann solvers, parameter vectors and difference schemes," Journal of Computational Physics **46**(2), 357–378 (1980) doi: 10.1016/0021-9991(81)90128-5.

[39] M. L. Shur, P. R. Spalart, and M. K. Strelets, "Noise prediction for increasingly complex jets. Part I: Methods and tests," International Journal of Aeroacoustics **4**(3), 213–246 (2005) doi: 10.1260/1475472054771376.

[40] P. R. Spalart, W. H. Jou, M. Strelets, and S. R. Allmaras, "Comments on the feasibility of les for wings, and on a hybrid rans/les approach," 1st AFOSR Int. Conf. on DNS/LES, Ruston, LA (1997).

[41] P. R. Spalart and S. R. Allmaras, "A one-equation turbulence model for aerodynamic flows," AIAA Paper 1992-0439 (1992) doi: 10.2514/6.1992-439.

[42]J. Xiong, F. Liu, and D. Papamoschou, "Large eddy simulation of three-stream jets," AIAA Paper 2018-1737 (2018) doi: 10.2514/6.2018-1737.

[43]J. Bridges, "Rapid prediction of installed jet noise from RANS," AIAA Paper 2019-2732 (2019) doi: 10.2514/6.2019-2732.

[44]A. Adam, D. Papamoschou, and C. Bogey, "The imprint of vortical structures on the pressure field at the edge of a turbulent high-speed jet," AIAA Paper 2021-1184 (2021) doi: 10.2514/6.2021-1184.

[45]D. Papamoschou, J. Xiong, and F. Liu, "Towards a low-cost wavepacket model of the jet noise source," AIAA Paper 2015-1006 (2015) doi: 10.2514/6.2015-1006.

[46]F. Coiffet, P. Jordan, J. Delville, Y. Gervais, and F. Ricaud, "Coherent structures in subsonic jets: A quasi-irrotational source mechanism?," International Journal of Aeroacoustics **5**(1), 67–89 (2006) doi: 10.1260/147547206775220407.